

# Venus wind map at cloud top level with the MTR/THEMIS visible spectrometer.

## I. Instrumental performance and first results.

Patrick Gaulme<sup>a</sup> François-Xavier Schmider<sup>b</sup> Catherine Grec<sup>b</sup>  
Arturo López Ariste<sup>c</sup> Thomas Widemann<sup>a</sup> Bernard Gelly<sup>c</sup>

<sup>a</sup>*LESIA, Observatoire de Paris, 5 place J. Janssen, F-92195 Meudon cedex*

<sup>b</sup>*Laboratoire Fizeau, Université de Nice Sophia-Antipolis, CNRS-Observatoire de  
la Côte d'Azur, F-06108 Nice cedex 2*

<sup>c</sup>*THEMIS Observatory, La Laguna, Tenerife, Spain*

---

### Abstract

Solar light gets scattered at cloud top level in Venus' atmosphere, in the visible range, which corresponds to the altitude of 67 km. We present Doppler velocity measurements performed with the high resolution spectrometer MTR of the Solar telescope THEMIS (Teide Observatory, Canary Island) on the sodium D2 solar line (5890 Å). Observations lasted only 49 min because of cloudy weather. However, we could assess the instrumental velocity sensitivity, 31 m s<sup>-1</sup> per pixel of 1 arcsec, and give a value of the amplitude of zonal wind at equator at 151 ± 16 m s<sup>-1</sup>.

*Key words:* Venus, Wind, Clouds, Visible, Spectrometry

*PACS:*

---

## 1 Introduction

ESA's Venus Express (VEx) space probe has been orbiting around Venus since April 2005. The mission's main goal is a better understanding of the atmospheric circulation, in particular of the wind super-rotation. The key questions regard the meridian circulation at top cloud level, the vertical extension of Hadley cells and the latitudinal dependance of the zonal wind. VEx obtains wind velocity map with cloud tracking and wind vertical profile from thermal wind maps. VEx measurements are limited by three factors. First, because of

---

*Email address:* Patrick.Gaulme@obspm.fr (Patrick Gaulme).

a very eccentric orbit, i.e. a strong velocity at periastron, VEx is not able to follow the motion of cloud features, at latitude above 20° N. Second, with cloud tracking, the temporal resolution cannot get lower than 1 h. At last, wind measurements are restricted to two levels, corresponding to cloud top, that is to say at 67 km on the day side and 50 km on the night side (Drossart et al. 2007). That is why, a large ground-based support has been organised around the 2007 Venus' maximum elongation in May-June and early November. The main idea was to get radial velocity measurements with spectrometry, almost simultaneously, in several spectral ranges in order to probe as many levels as possible of the upper atmosphere.

Hereafter, we present spectrometric measurements on the sodium D2 solar line (5890 Å), lead at THEMIS solar telescope (Teide Observatory, Canary Islands), on discretionary time, on November 7th 2007. The objective of this run was the evaluation of instrumental performance of the MTR spectrometer, for radial velocity measurements on a planetary target. The advantage of MTR/THEMIS spectrometer with respect to point to point echelle-spectrometer measurements is the ability to build velocity maps, using a long slit entrance, greater than planetary diameter, which allows us to scan completely the whole planet with only 15 positions of the slit. Because of cloudy weather, observations lasted only 49 min. However, it is enough to evaluate the signal to noise level and to give an estimate of the zonal wind velocity. We present the instrument main properties (Sect. 2), the data processing (Sect. 3) and, then, the estimate of the instrumental performance and velocity field (Sect. 4).

## 2 Instrument main characteristics, observing conditions and expected performance

### 2.1 MTR-THEMIS high resolution spectrometer

THEMIS (Télescope Héliographique pour l'Etude du Magnétisme et des Instabilités Solaires) is a French-Italian solar telescope dedicated to accurate measurement of polarisation of solar spectral lines, with high spatial, spectral and temporal resolutions (Mein & Rayrole 1985). It is a 90-cm diameter Ritchey-Chrétien telescope. For present observations, it has been operated in the MTR (MulTiRaies) mode (Rayrole & Mein 1993) which allows spectropolarimetric observations in up to 6 different spectral domains simultaneously. For radial velocity measurements, the polarimetric analysis was skipped and only spectrometric information is considered. For this test run, we used the existing setup of the instrument and focused on the sodium D2 solar line (5890 Å). It is one of the deeper lines in the optimal spectral domain for MTR de-

tectors, but it is not optimum for Doppler sensitivity. We might search for a better line for future observations.

## 2.2 Observing conditions

Data were acquired on November 7th, 2007 between 13:06:52 h and 13:55:34 h (UT). The slit entrance dimension was about  $(0.5 \times 100)$  arcsec. The spectral resolution was about 20 mÅ, while the seeing has been estimated to 1 arcsec. The detector is a  $512 \times 512$  pixels CCD. The spatial dispersion upon the detector was equal to 0.2 arcsec pixel<sup>-1</sup> and the spectral dispersion was equal to 11.7 mÅ pixel<sup>-1</sup>. The exposure time has been set to 10 s, while the readout time was less than 50 ms per exposure. We have considered the latter as negligible.

The planet's diameter was about 21.76 arcsec and the phase angle about 83.59° (Fig 1), which was close to maximum elongation (on October 27th, 2007). Only 15 scans regularly spaced of about 0.8 arcsec were necessary to map the whole enlightened part of the planet. However, because of bad weather conditions, the scanning schedule got changed and did not work nicely. In particular, no dark field nor flat field were done and the scanning was off. The guiding was manually set on Venus' limb, and the positioning upon the disk slowly drifted along the run. Therefore, the planetary scan was only due to the drift of the planet inside the field of view, which has limited the coverage to 70 % of the radius, i.e. an extension of about 8 arcsec along the equator (Fig. 2). Nevertheless, 318 spectra were obtained in the 49-minute observation run. Observing conditions were satisfactory during acquisition as illustrated by the stability of the mean intensity of the terrestrial signal (Fig. 3). We could evaluate the instrumental performance and estimate qualitatively the velocity range along the scan. The terminator region, where the sun-Venus Doppler effect is expected to be maximum, is covered by the observation. Expected performance and detailed analysis are presented in next sections.

## 2.3 Theoretical performance

The principle of our observations rests on the measurement of the position of a solar Fraunhofer line (D2, sodium), which gets shifted by Doppler effect after reflection on Venus cloud decks. The radial velocity sensitivity depends on the sodium line thickness and the total amount of photons. First, measured on highly resolved spectrum, the local slope of the D2 sodium line appears to be  $(\delta I/I)_{\text{max}} = 10^{-4}$  per m s<sup>-1</sup> at maximum, or, in average  $\langle \delta I/I \rangle = 0.5 \cdot 10^{-4}$  per m s<sup>-1</sup> for two 60 mÅ bandwidths at each side of the line (see Fig. 4). Second, knowing that Venus emits almost  $4.8 \cdot 10^{11}$  photons s<sup>-1</sup> m<sup>-2</sup> (1000 Å)<sup>-1</sup>

in the visible range on a 187-arcsec square lighted surface, that the telescope's efficient surface is about  $0.5 \text{ m}^2$ , that the slit width is open at 0.5 arcsec, and that the global transmission is about 5 % at  $5500 \text{ \AA}$ , we expect  $1156 \text{ photons s}^{-1} \text{ arcsec}^{-2}$  on Venus. Since the total duration of the run is about 49 min and the spatial extension of the observed zone is about 8 arcsec, almost 6.1 min are dedicated per each 1-arcsec position of the slit, i.e. for each Venus slab. Consequently, the total amount of photons per 1 arcsec square is almost  $4.23 \cdot 10^5$ , that is to say a signal to noise ratio  $\text{SNR} \simeq 650$ . Therefore, the expected  $1\text{-}\sigma$  velocity sensitivity is about  $1/(650 \times 0.5 \cdot 10^{-4}) = 30.7 \text{ m s}^{-1}$  per pixels of 1 arcsec square.

### 3 Data analysis

#### 3.1 Cleaning out raw spectra

Fig. 5 presents a typical raw spectrum obtained on Venus. Y-axis corresponds to spatial dimension, parallel to the terminator, and  $x$ -axis corresponds to spectral dimension. The spatial range corresponds to 100 arcsec and the total spectral range to  $6 \text{ \AA}$ . Since the entrance slit is much larger than the planetary diameter, most of the image is occupied by solar radiation scattered by Earth's atmosphere. The Doppler shift of the D2 sodium line between Venus and Earth atmosphere is clearly visible at image center on Fig. 5 (left). Thinner lines crossing vertically the detector are telluric absorption lines. A slight distorsion is visible across the field. This is a consequence of the optical design of the spectrometer. At first order, distorsion parameters can be considered uniform across the field. We calculate them by fitting the Earth's D2 sodium line with a second order polynomial. The distorsion is then rectified with a cubic spline interpolation algorithm. This effect is purely instrumental. Distorsion can be considered constant through the observation run, so the fit has to be performed only once, on one image. The same correction algorithm is applied to all spectra.

#### 3.2 Positioning on the planetary disk

The main cause of uncertainty in processing the data comes from the positioning on the disk. Indeed, as the quick scan of the planet did not work, we have no direct measurement of the absolute position. The positioning is determined as a relative function of the initial pointing along the terminator. The spatial scale is determined using the spatial extension of Venus on first spectra, which covers 115 pixels, and fits the expected diameter of Venus upon the detector

119  $(21.76 \times 0.2 = 109 \text{ pixel})$ , taking into account the seeing effect. If we suppose  
 120 that the slit slewed parallel to the terminator, the positioning upon the planet  
 121 only depends on the ratio of the measured cut along the planet with respect  
 122 to its size at terminator.

$$123 \quad x_{\text{eq}} = \cos \theta \quad \text{with} \quad \theta = C/D_{\text{venus}} \quad (1)$$

124 where  $x_{\text{eq}}$  indicates the  $x$ -coordinate along the planetary equator,  $\theta$  the lati-  
 125 tude,  $C$  the extension of the planetary cut (pixels) and  $D_{\text{venus}}$  Venus measured  
 126 diameter (pixels) (see Fig 2). Note that this expression assumes that Venus  
 127 was at quadrature (phase angle  $90^\circ$ ) and the central meridian is the termina-  
 128 tor. The phase angle was  $84^\circ$  instead of  $90^\circ$ , yielding a difference of 1.1 arcsec,  
 129 that is the spatial resolution by taking into account the seeing.

130 The spatial extension of Venus on the detector is determined after subtraction  
 131 of Earth's skylight mean signal (Fig 5). Then, the spectral image is projected  
 132 along the  $y$ -axis, in order to get a smooth spatial profile. Venus' spatial dimen-  
 133 sion is arbitrarily defined as the region where the intensity exceeds the 1/2 of  
 134 the maximum value, i. e. the full width at half maximum (FWHM) (see Fig  
 135 6). We estimate the spatial extension at half maximum in order to minimize  
 136 error due to seeing fluctuations, as illustrated by Fig. 6.

137 Plotting the FWHM as a function of time shows a slow drift, overlapped by  
 138 a high frequency oscillation (Fig. 7). Such fluctuations are due to the bias  
 139 introduced by rapid seeing (10-s interval from one image to another). The  
 140 fit value used to calculate the position upon the planetary disk is obtained by  
 141 a 3rd order polynomial. The standard deviation of the points with respect to  
 142 their smoothed profile is about 2.46 pixels, which corresponds to 0.49 arcsec.  
 143 This gives us the relative error bar of the slit position estimate  $x_{\text{eq}}$  on the disk  
 144 (Fig. 2).

### 145 3.3 Doppler shift of D2 lines

146 Doppler maps are obtained by measuring the shift between the D2 sodium  
 147 lines, scattered by Earth's and Venus' atmospheres. The shift must first be  
 148 corrected from (i) Venus' center motion with respect to observer and (ii) ob-  
 149 server's motion with respect to the Sun. All these components are well known,  
 150 and get subtracted with the help of ephemeris data (Fig. 8).

151 The Earth scattered solar D2 line intensity is averaged over all detector lines  
 152 outside of Venus, to create a mean reference spectrum. On Venus, the 0.2-  
 153 arcsec lines are coadded by groups of 5 in order to reach a 1-arcsec vertical  
 154 resolution along the slit, thus improving the signal to noise ratio by a factor

155  $\sqrt{5}$ . The reference spectrum is then correlated to the spectrum measured on  
156 Venus, line by line; the Doppler shift corresponds to the position of maximum  
157 value of the cross correlation. Points are fitted with a 4th order polynomial,  
158 then, the maximum position is determined by calculating numerically the zeros  
159 of the derivative of the fitting function (Fig 9). The fit accuracy is strongly de-  
160 pendent upon S/N; that is why we consider only the signal coming from Venus  
161 central region on the detector, where amplitude is greater than half maximum  
162 amplitude, as for the cut estimate (previous Sect.). In terms of angular size,  
163 it means to keep 16 arcsec instead of 21.8 arcsec along the diameter; in terms  
164 of latitude, it limits the map to  $\pm 45^\circ$ .

165 The global measurement of the Doppler shift is represented in a spatial-  
166 temporal diagram on Fig. 10, top left. Although the scan motion was perpen-  
167 dicular to terminator, we note that the upper edge of the planet is a straight  
168 line, whereas the bottom edge is curved. This is due to the fact that man-  
169 ual guiding was performed on the top of Venus image in the field (southern  
170 hemisphere). This guiding procedure and resulting vertical drift allowed us to  
171 reveal a spectral artifact probably due to the missing calibration procedures  
172 we referred to in section 2, §2.3. This spectral artifact is visible on Fig. 10,  
173 top left frame, as a white horizontal band between  $y = 40$  and  $y = 45$  arcsec.  
174 We decided to pursue the analysis by trying to correct it the following way.  
175 First, we coadded all the lines to assess the mean variation of the Doppler  
176 integrated over slit height. This mean variation is shown in Fig. 10, bottom.  
177 It shows qualitatively that the spectral shift between Earth's solar D2 and  
178 Venus' solar D2 decreases as the slit moves away from terminator. This aver-  
179 age decrease is then fitted to a weighted moving average in order to flatten the  
180 Doppler surface, with respect to time, prior to the kinematical fit described  
181 in Section 4. Second, the temporal mean of this diagram, shown in Fig. 10,  
182 right frame, has been subtracted to the main data frame in order to remove  
183 the artifact. The result is shown in Fig. 11.

## 184 4 Results

### 185 4.1 Working with relative velocities

186 Strong discrepancies of up to several tens of  $\text{m s}^{-1}$  have been commonly met  
187 with tentatives of making absolute radial velocity measures using visible lines.  
188 This has been discussed in the case of Venus wind measurements in Young  
189 et al. (1979), Widemann et al. (2007, 2008). These authors concluded for the  
190 need of a reference point on Venus used as a relative velocity reference, and  
191 they used this point to perform differential velocity measurements on the disk.  
192 The 0 velocity is fixed at the planetary coordinates ( $\theta = 0^\circ, \alpha = 5^\circ$ ), where  $\theta$

193 and  $\alpha$  indicate the latitude and longitude.

194 The radial velocity map is shown in Fig. 12. The maximum velocity difference  
195 on the whole map reaches almost  $300 \text{ m s}^{-1}$ , while the mean amplitude of the  
196 variation of velocity across the planet is about  $200 \text{ m s}^{-1}$ . A rough estimate  
197 of the actual mean noise level can be obtained by measuring the standard  
198 deviation  $\Sigma$  of each “column of pixels” on Venus figure. The mean value of  
199 the dispersion of points along a column is equal to  $31 \text{ m s}^{-1}$  (see Tab 2). Note  
200 that the higher noise level, which is observed in column of abscissa  $x = [5, 6]$ ,  
201 is due to a geometrical effect. Indeed, the wind velocity on Venus varies more  
202 strongly in columns far from the terminator, because a wide range of longitude  
203 is explored, what increases the standard deviation of the considered column.  
204 This fact makes the mean standard deviation value appear as a slightly pes-  
205 simistic estimate of the actual mean noise level per pixel. Nevertheless, its  
206 value, about  $31 \text{ m s}^{-1}$ , almost squares with the theoretical performance ( $30.7$   
207  $\text{m s}^{-1}$ ) presented in Sect. 2.3, what shows that our estimate of the noise level  
208 is correct.

#### 209 4.2 *Fit of Doppler winds to zonal circulation*

210 Doppler blueshift between Venus’ atmosphere and the Sun is maximum along  
211 the terminator, whereas Doppler redshift between Earth and Venus is maxi-  
212 mum along the planetary limb. By supposing a purely zonal wind, the isotach  
213 corresponding to radial velocity  $v_{\text{rad}} = 0$  is the meridian defined by the bisect-  
214 ing angle between sub-earth and sub-solar longitudes. Moreover, a correction  
215 has been introduced by Young et al. (1979), taking into account the solar ap-  
216 parent diameter and its rotation seen from Venus (42 arcmin), so-called *Young*  
217 *effect* (see also Widemann et al., this issue).

218 The consequence is an increase of the apparent Doppler shift for the observer,  
219 along the terminator at mid and high latitudes ( $\pm 45^\circ$ ). The typical amplitude  
220 of the wind increase reaches almost  $30 \text{ m s}^{-1}$  for a  $100 \text{ m s}^{-1}$  zonal wind, and  
221 therefore must be arbitrarily corrected in a kinematical fit to a pure zonal  
222 regime.

223 The algorithm used to extract the velocity amplitude from the radial velocity  
224 map has been adapted from Widemann et al. (2007). The zonal circulation  
225 at cloud top level is characterized by a latitudinal dependency and wind de-  
226 crease in the polar regions. Recently reanalysed Pioneer Venus UV data (Li-  
227 maye, 2007) and SSI Galileo imaging (Peralta et al. 2007) indicate a generally  
228 uniform velocity between latitude  $\pm 50^\circ$  with a best fit to a constant angular  
229 velocity at higher latitudes, in accordance with winds measured from cloud  
230 tracking by both VIRTIS-M and VMC (Markiewicz et al., 2007 ; Piccioni et

231 al., 2007). Both types of zonal wind regimes dependency have been applied to  
232 fit our data using classical least-square algorithm.

233 For a uniform, solid body circulation, the wind velocity is estimated at at  $2\sigma$   
234 at  $151 \pm 16 \text{ m s}^{-1}$ , with reduced  $\chi^2 = 1.69$ . On the other hand, with a cosine  
235 latitudinal dependance, the zonal wind velocity is estimated at  $146 \pm 17 \text{ m s}^{-1}$ ,  
236 with reduced  $\chi^2 = 1.85$ . The close results between the two approaches is due to  
237 the fact that our observations do not explore (with good SNR) Venus wind map  
238 at latitude higher than  $45^\circ$ . Under this latitude, the difference between both  
239 models is not very significant. It has to be noticed that uncertainties on the  
240 wind global velocity ( $16\text{-}17 \text{ m s}^{-1}$ ) is larger than what would be expected from  
241 local noise level. Indeed, with a local noise level of  $31 \text{ m s}^{-1}$  per 1 arcsec square  
242 pixel on about 128 pixels, the global noise level by integrating all Venus' pixels  
243 would decrease to  $31/\sqrt{128} = 2.7 \text{ m s}^{-1}$ . This lower performance is due to three  
244 facts. First, the sensitivity of Doppler measurements to velocity is not uniform  
245 on the planet (isotachs are functions of longitude, e. g. Widemann et al. 2007).  
246 Second, the real velocity field might not be uniform as supposed inside the  
247 model used to fit the data. At last, the previously exposed uncertainty about  
248 the positioning introduces a bias in the global fit.

249 Our result is compatible with Doppler spectroscopy measurements of Wide-  
250 mann et al. (2007), where the wind amplitude is estimated in a  $[90, 150] \text{ m}$   
251  $\text{s}^{-1}$  velocity range. However, this result represents an upper value with respect  
252 to VEx results of Markiewicz et al. (2007), who have obtained a mean value  
253 zonal wind of  $95 \text{ m/s}$  between latitudes  $10\text{N}$  and  $40\text{S}$ , using cloud tracking  
254 method. Two reasons may explain the discrepancy between our results and  
255 those of Markiewicz et al. (2007). First, it could be a consequence of the un-  
256 certainty on the positioning, what would implies a  $60\text{-m s}^{-1}$  bias in global  
257 velocity estimate. Second, it might point out the fact that cloud tracking and  
258 Doppler spectrometry are two distinct approaches to measure the wind veloc-  
259 ity. With cloud tracking, one measure the cloud feature motion, while Doppler  
260 spectrometry measures the cloud particle motion, which may differ.

## 261 5 Conclusions and prospects

262 The goal of our observations was to evaluate the ability of the MTR/THEMIS  
263 solar telescope in order to measure velocity wind by Doppler spectroscopy  
264 in the visible range. Despite cloudy weather, and consequently a very short  
265 run (49 min), we obtain a promising instrumental performance: the mean  
266 noise level on the velocity map is about  $31 \text{ m s}^{-1}$  per 1-arcsec pixel, which  
267 corresponds to the expectations. As regards the wind velocity field, it has been  
268 estimated at  $149 \pm 16 \text{ m s}^{-1}$ , what represents a quiet excessive value with  
269 respect to other observations. We have given two possible explanations. First,



270 it could come from a global bias introduced by the observation conditions, in  
 271 particular to the lack of quick scan, which has made the positioning upon the  
 272 planetary disk noisy. Also, It might be due to the fact that cloud tracking  
 273 and Doppler measurements represent different approaches to wind velocity  
 274 estimate. Part of this spurious velocity which has be seen in fig. 10 would be  
 275 skipped out with the use of the tip-tilt guiding system and by optimizing the  
 276 instrumental configuration. By supposing the same local noise level ( $31 \text{ m s}^{-1}$ )  
 277 and by choosing Fraunhofer lines with a better sensitivity to Doppler shifts,  
 278 it would be possible to reach a noise level around  $10 \text{ m s}^{-1}$  per 1 arcsec square  
 279 in few hour observation run and to reach a global wind measurement accuracy  
 280 of about several  $\text{m s}^{-1}$ .

281 These encouraging performance have motivated a new observation campaign,  
 282 which is planned for mid spring 2008. Tip tilt guiding will be used. Venus will  
 283 present a shorter apparent diameter (10 arcsec) and a greater phase (90 %).  
 284 Four deep solar lines will be used to measure velocity fields (Fe I, Mg, D1 and  
 285 D2 Na), in order to gain a factor 2 in the SNR. Moreover, the Doppler shift  
 286 of  $\text{CO}_2$  line ( $\nu_3$  band,  $8680 \text{ \AA}$ ) will be studied in order to probe 7 km higher.  
 287 Future observations will be of major interest because at short elongation Venus  
 288 is practically unobservable with classical night telescopes, whereas VEx is still  
 289 orbiting around Venus.

## 290 References

- 291 [1] Drossart, P. Piccioni, G., Adriani, . et al. 2007. Scientific goals for the observation  
 292 of Venus by VIRTIS on ESA/Venus Express mission. Planet. Sp. Sci. 55, P. 1653.
- 293 [2] Gierasch, P. J.; Goody, R. M.; Young, R. E.; and 10 co-authors, 1997. The  
 294 General Circulation of the Venus Atmosphere: an Assessment. Venus II :  
 295 Geology, Geophysics, Atmosphere, and Solar Wind Environment. University  
 296 of Arizona Press, p.459
- 297 [3] Lellouch, E., T. Clancy, D. Crisp, A.J. Kliore, D. Titov, And S.W. Bougher  
 298 1997, Monitoring of Mesospheric Structure and Dynamics, Venus II, S.W.  
 299 Bougher, D.M. Hunten, & R.J. Phillips eds., University of Arizona Press,  
 300 Tucson, 295-324.
- 301 [4] Limaye, S. S. 2007. Venus atmospheric circulation: known and unknown. JGR  
 302 112, p. 4.
- 303 [5] Markiewicz, W. J.; Titov, D. V.; Limaye, S. S.; and 7 co-authors, 2007.  
 304 Morphology and dynamics of the upper cloud layer of Venus. Nature, Volume  
 305 450, Issue 7170, pp. 633-636
- 306 [6] Mein, P.; Rayrole, J., 1985. Themis solar telescope. Vistas in Astronomy, vol.  
 307 28, Issue 2, pp.567-569

- 308 [7] Peralta, J.; Hueso, R.; Snchez-Lavega, A. 2007. A reanalysis of Venus winds  
309 at two cloud levels from Galileo SSI images. *Icarus*, Volume 190, Issue 2, p.  
310 469-477.
- 311 [8] Piccioni, G.; Drossart, P.; Sanchez-Lavega, A. and 102 co-authors. A dynamic  
312 upper atmosphere of Venus as revealed by VIRTIS on Venus Express. *Nature*,  
313 Volume 450, Issue 7170, pp. 641-645.
- 314 [9] Rayrole, J.; Mein, P., 1994. THEMIS Telescope: Prospects in High Resolution  
315 Magnetic Field Observations. *IAU Colloquium no. 141*, p.170
- 316 [10] Widemann, T.; Lellouch, E.; Campargue, A., 2007. New wind measurements in  
317 Venus lower mesosphere from visible spectroscopy. *Planetary and Space Science*,  
318 Volume 55, Issue 12, p. 1741-1756.
- 319 [11] Widemann, T.; Lellouch, E.; Donati, J.-F., 2008, Venus Doppler winds observed  
320 at cloud tops with Espadons at CFHT, this issue.
- 321 [12] Young, A. T.; Schorn, R. A.; Young, L. D. G.; Crisp, D., 1979. Spectroscopic  
322 observations of winds on Venus. I - Technique and data reduction. *Icarus*, vol.  
323 38, p. 435-450

Table 1

Observation properties of Venus on November 7th 2008 from Teide Observatory (IMCCE ephemeris database).

Date UTC	R.A	Dec.	Distance	V.Mag	Phase	Dist dot
h m s	h m s	o ' "	ua.		o	o
13 6 0.00	11 56 21.86	01 28 42.10	0.77	-4.31	83.58	13.27725
13 56 0.00	11 56 30.16	01 27 57.89	0.77	-4.31	83.56	13.32962

Table 2

Standard deviation  $\Sigma$  of velocity in each column of the Venus map. The mean standard deviation value is equal to  $31 \text{ m s}^{-1}$ . The third line indicate the number of spectra averaged in order to build each column. We have averaged column 11 and 12 because column 11 alone have only 5 spectra, which affect the global noise level. The standard deviation increases in column 5 and 6 and 7 despite a major number of averaged spectra, because of the wind velocity strong variation in these columns.

Abcissa $x$	(12,11)	10	9	8	7	6	5
$\Sigma \text{ (m s}^{-1}\text{)}$	42.96	27.60	25.06	23.93	30.27	33.00	34.72
Number of spectra	30	31	40	48	56	67	43

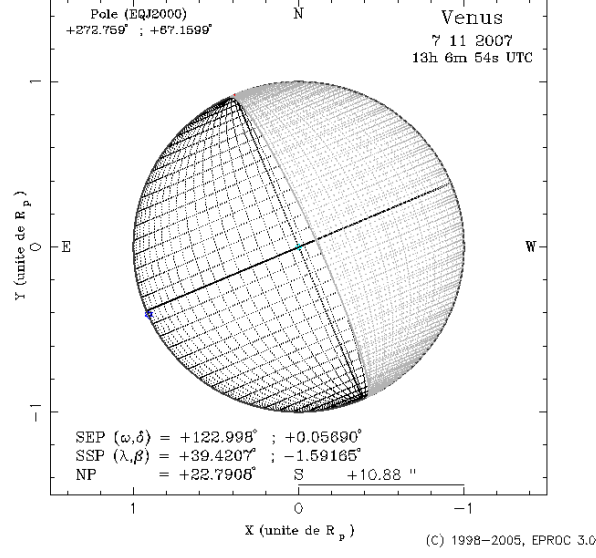


Fig. 1. Venus appearance during observations, on November 7th, 2007 at 13:06:54 h (UTC). The planetary radius is about 10.88 arcsec and the phase angle about  $83.59^\circ$ . SEP and SSP stand for sub-Earth point and sub-solar point.

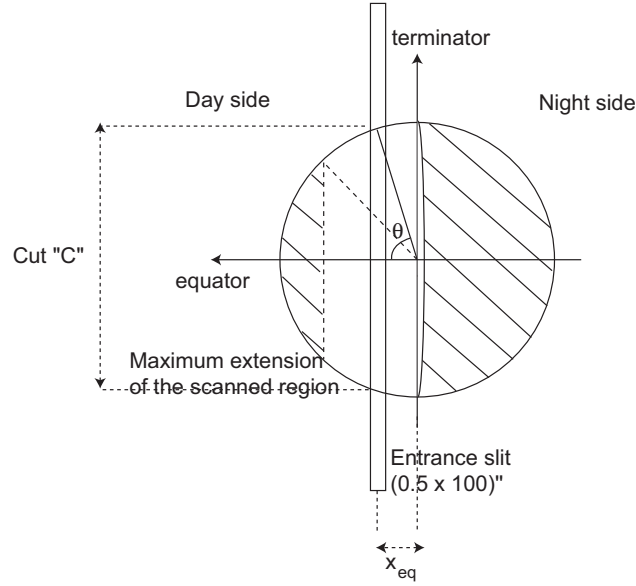


Fig. 2. Schematic review of notations used in this paper and illustration of the spatial coverage of Venus by our observations. The slanted lines indicate the region which is not covered by observations.  $\theta$  indicates the latitude and  $C$  the cut along the planet, through the entrance slit (in pixels). The maximum extension of the spatial coverage reaches  $\theta = 45^\circ$  on the planetary limb.

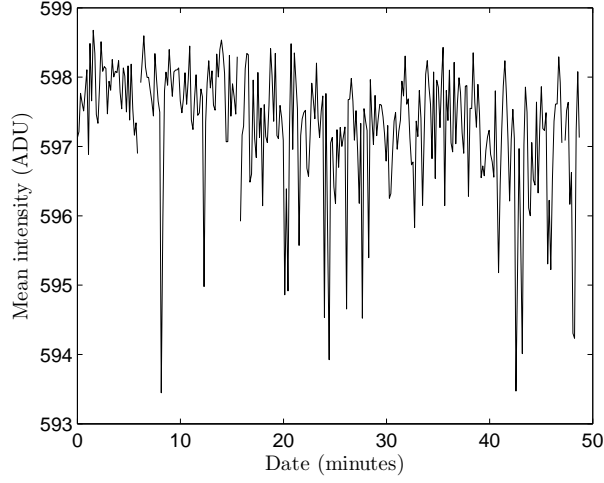


Fig. 3. Mean intensity measured on Earth's skylight background on each spectrum of the temporal series. The mean value is equal to 597.6 ADU, whereas the standard deviation of the points is equal to  $\Sigma = 58.16$  ADU.

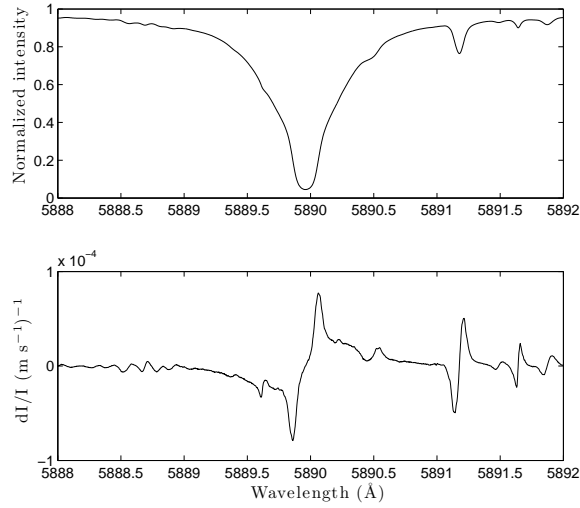


Fig. 4. Top: D2 sodium line on Sun spectrum as function of the wavelength (BASS 2000 database, <http://bass2000.obspm.fr>). Intensity has been normalized to 1. The Doppler sensitivity is related to the slope of the considered line. It reaches its maximum at the transmission level of 30%. Bottom: the slope of the upper figure, converted in meter per second. In average, the Doppler velocity sensitivity is about  $\langle \delta I/I \rangle = 0.5 \cdot 10^{-4}$  per  $\text{m s}^{-1}$  for a bandwidth of 60 mÅ.

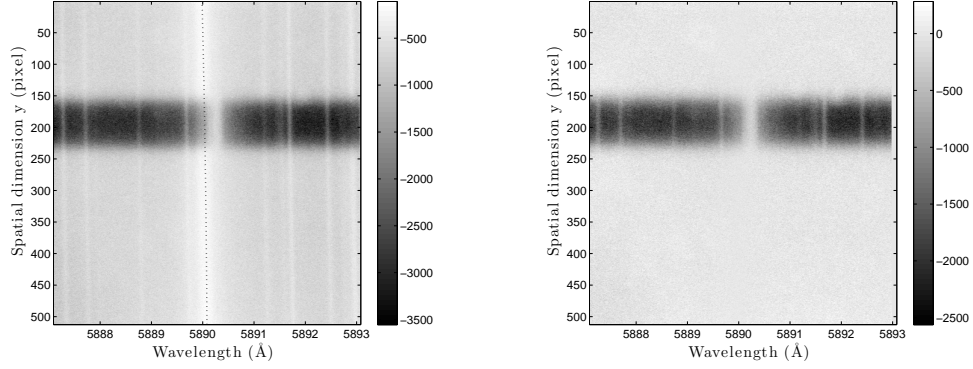


Fig. 5. Left: raw spectrum of Venus, centered on D2 sodium solar line. The  $y$ -axis corresponds the spatial dimension, while the  $x$ -axis squares with the spectral dimension. Venus corresponds to the dark region on the detector, with highest intensity, whereas the light background corresponds to the Earth's sky spectrum. The D2 line on Venus is clearly shifted with respect to the Earth's. The slight curvature across the whole image is estimated by fitting the D2 sodium line scattered by Earth's atmosphere with a second order polynomial (dot line). Right: clean spectrum. After straightening out the distortion, skylight sodium light has been averaged over the background, and subtracted to Venus. Thinner lines correspond to telluric absorption lines.

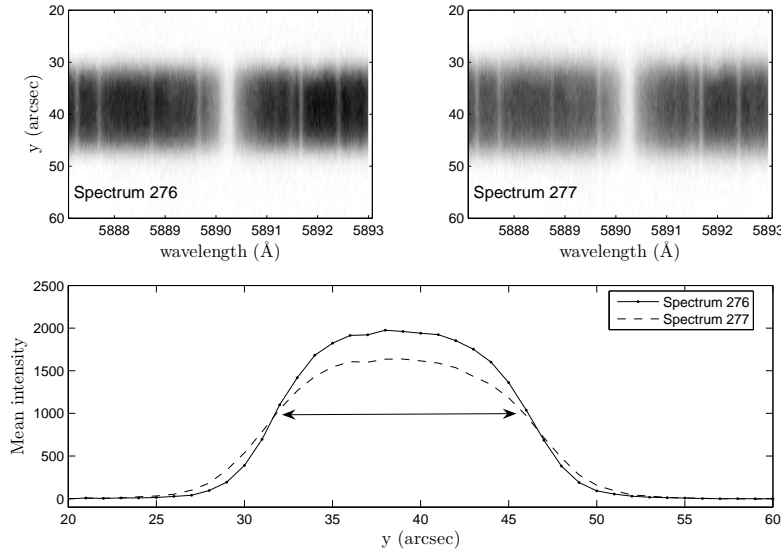


Fig. 6. Top: two consecutive spectra (labelled 276 and 277 among the 318 spectra temporal series), which have been acquired with an interval of 10 s. Bottom: projection of both spectra along the  $y$ -axis, in order to evaluate the spatial extension of the planet selected by the entrance slit. Width determination is the only method to locate the slit projection on Venus.

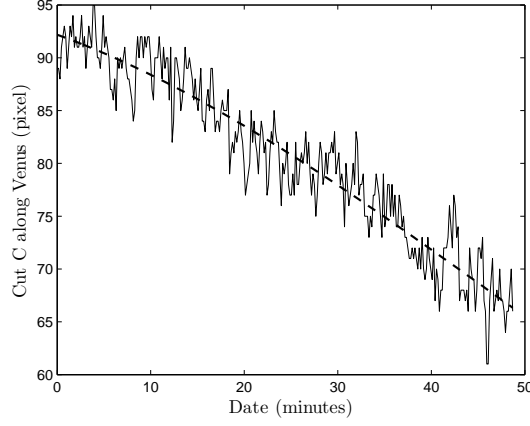


Fig. 7. Spatial extension estimate “C” as function of time, along the observation run. The cut extension has been calculated on full resolution images, in order to keep the original accuracy; 1 pixel corresponds to 0.2 arcsec. The extension is defined by the width at half maximum. The solid line represents the measurement of the spatial extension, while the dashed line represents the polynomial fitting of Venus cut. The standard deviation of points around the mean is equal to 2.46 pixels.

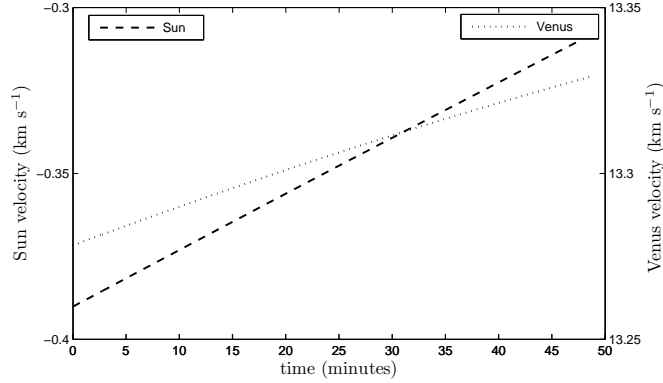


Fig. 8. Relative velocities with respect to Teide Observatory between 13:06:52 h and 13:55:34 h (UT) on November, 7th 2007. Initial date squares with 13:06:00 h, velocities are expressed in  $\text{km s}^{-1}$ . Left  $y$ -axis indicates Sun relative velocity, which mean amplitude is about  $-0.35 \text{ km s}^{-1}$ . Right  $y$ -axis indicates Venus relative velocity, which mean is about  $+13.3 \text{ km s}^{-1}$ . Consequently, the mean Doppler shift between D2 sodium line scattered by Venus’ and Earth’ atmospheres is equal to  $+13.65 \text{ km s}^{-1}$  ([www.imcce.fr](http://www.imcce.fr)).

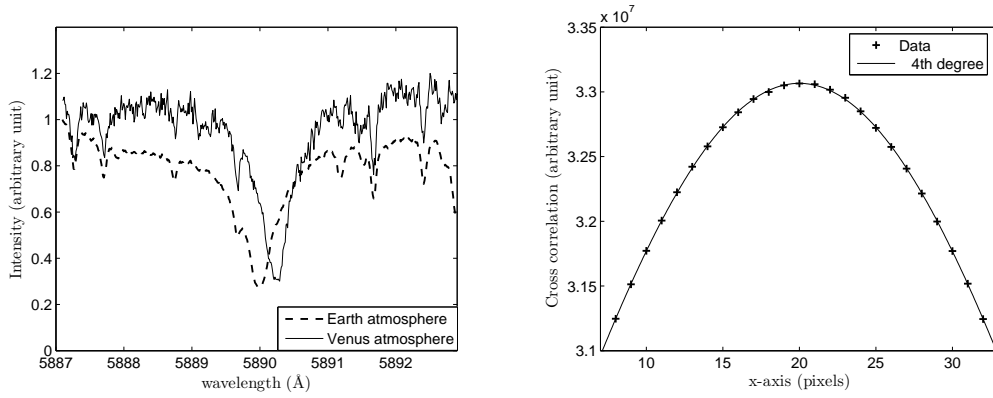


Fig. 9. Left: reference mean spectrum (dashed line) and Venus spectrum as a function of the wavelength (full line). Reference spectrum is calculated for each spectrum by averaging all the skylight spectrum. Venus spectrum is obtained on a 1 arcsec spatial resolution spectrum, and correspond to the planetary equator. Both spectrum have been normalized with respect to their maximum value and Venus spectrum has been offset, only for graphical reasons. Right: 4th order polynomial fit of the maximum of the cross correlation between Venus and reference spectra. The Maximum position is equal to 20.51 pixels.

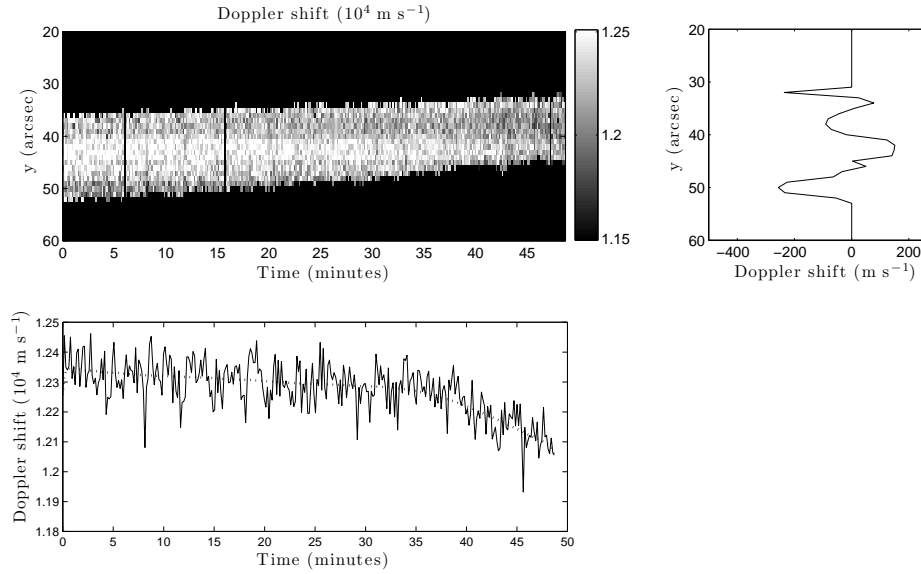


Fig. 10. Top left: Doppler shift diagram as a function of time ( $x$ -axis) and space ( $y$ -axis). Doppler shift is expressed in  $10^4 \text{ m s}^{-1}$ . Bottom left: mean Doppler shift with time. Top right: mean Doppler shift with spatial dimension. The dashed line on the bottom left plot indicates the fitted estimate obtained by a weighted moving average, which has been used to characterize the vertical distortion of the Doppler “surface” plotted in bottom right figure.



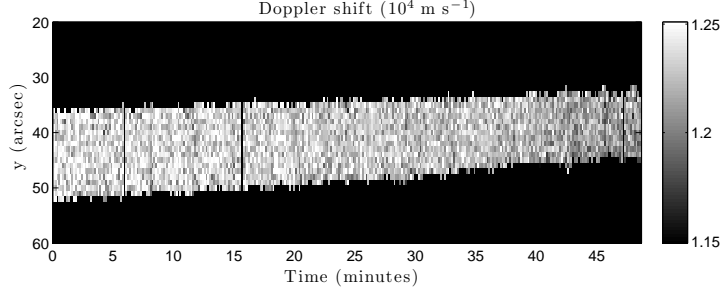


Fig. 11. Clean Doppler diagram, obtained after subtraction of the spurious distorted “surface” enlightened in the raw diagram (Fig 10).

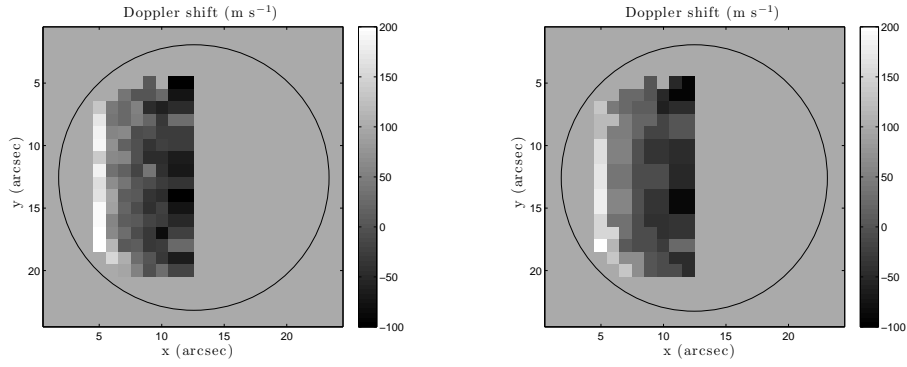


Fig. 12. Left: Relative velocity map obtained after summation of Doppler shift within 1-arcsec intervals. The dot line circle indicates the planetary diameter. The maximum latitude extension reaches  $\pm 45^\circ$ , while the maximum longitude reaches 55 at pixels (5, 7) and (5, 17). Right: the same Doppler map where pixels have been averaged within a regular latitude-longitude grid, spaced by  $10^\circ$ . Latitude range is  $[-45^\circ, 45^\circ]$  while longitude range is  $[0^\circ, 55^\circ]$ .

